Available online at www.sciencedirect.com

ScienceDirect

Geochimica et Cosmochimica Acta 181 (2016) 164–174

Geochimica et Cosmochimica Acta

www.elsevier.com/locate/gca

Water activities of $NaClO_4$, $Ca(ClO_4)_2$, and $Mg(ClO_4)_2$ brines from experimental heat capacities: Water activity >0.6 below 200 K

J.D. Toner *, D.C. Catling

University of Washington, Box 351310, Dept. Earth & Space Sciences, Seattle, WA 98195, USA

Received 11 December 2015; accepted in revised form 6 March 2016; Available online 10 March 2016

Abstract

Perchlorate salts found on Mars are extremely hygroscopic and form low eutectic temperature aqueous solutions, which could allow liquid water to exist on Mars despite cold and dry conditions. The formation, dynamics, and potential habitability of perchlorate salt solutions can be broadly understood in terms of water activity. Water activity controls condensation and evaporation of water vapor in brines, deliquescence and efflorescence of crystalline salts, and ice formation during freezing. Furthermore, water activity is a basic parameter defining the habitability of aqueous solutions. Despite the importance of water activity, its value in perchlorate solutions has only been measured at 298.15 K and at the freezing point of water. To address this lack of data, we have determined water activities in $NaClO_4$, $Ca(ClO_4)_2$, and $Mg(ClO_4)_2$ solutions using experimental heat capacities measured by Differential Scanning Calorimetry. Our results include concentrations up to near-saturation and temperatures ranging from 298.15 to 178 K. We find that water activities in $NaClO_4$ solutions increase with decreasing temperature, by as much as 0.25 a_w from 298.15 to 178 K. Consequently, a_w reaches ~0.6–0.7 even for concentrations up to 15 molal $NaClO_4$ below 200 K. In contrast, water activities in $Ca(ClO_4)_2$ and $Mg(ClO_4)_2$ solutions generally decrease with decreasing temperature. The temperature dependence of water activity indicates that low-temperature $NaClO_4$ solutions will evaporate and deliquesce at higher relative humidity, crystallize ice at higher temperature, and potentially be more habitable for life (at least in terms of water activity) compared to solutions at 298.15 K. The opposite effects occur in $Ca(ClO_4)_2$ and $Mg(ClO_4)_2$ solutions.

1. INTRODUCTION

The discovery of perchlorate (ClO_4^-) by the Phoenix Wet Chemistry Laboratory (WCL) (Hecht et al., 2009) has profoundly influenced our view of liquid water on Mars. Perchlorate salts can absorb water from the atmosphere to form brines (Gough et al., 2011), and once formed, such brines can remain liquid down to 195 K (Chevrier et al., 2009; Marion et al., 2010) or even lower (down to 150 K) due to supercooling (Toner et al., 2014a). These properties suggest that liquid water could form on present-day Mars despite extremely cold and dry conditions. Liquid water in the form of perchlorate brine has been invoked to explain Recurring Slope Lineae (RSL) (Chevrier and Rivera-Valentin, 2012; Ojha et al., 2015; Stillman et al., 2016) and the flow of Martian polar ice (Fisher et al., 2010; Lenferink et al., 2013). Perchlorate brines may even support extremophile forms of life (Coates and Achenbach, 2004; Davila et al., 2010).

The activity of water (a_w) is fundamental for understanding the formation and habitability of brines on Mars. Water activity is defined as the equilibrium fugacity of

* Corresponding author. Tel.: +1 267 604 3488.
E-mail address: toner2@uw.edu (J.D. Toner).

http://dx.doi.org/10.1016/j.gca.2016.03.005
0016-7037/

water vapor over a solution (f) relative to the fugacity of water vapor over pure water (f_0) ($a_w = f/f_0$). At low pressures, fugacities are well approximated by partial vapor pressures (p and p_0), leading to the more common expression $a_w \approx p/p_0$, which is equivalent to the equilibrium relative humidity (RH) over a salt solution ($RH_{eq} = a_w$). The exchange of water between a salt solution and the atmosphere is controlled by the relative values of RH and a_w: a solution will condense water from the atmosphere when $a_w < RH$, and it will evaporate when $a_w > RH$. Furthermore, crystalline salts will deliquesce when RH increases above a_w in the saturated salt solution ($a_{w,sat}$), and will effloresce (precipitate salt) when $RH < a_{w,sat}$, although kinetic effects often occur (Gough et al., 2011; Toner et al., 2014a). With respect to freezing, a_w at the freezing-point of ice is a well-known function of temperature, and can be used to predict the temperature at which ice crystallizes or melts in solution (Murphy and Koop, 2005). Finally, a_w measures how available water is for life to use, and is a basic criteria used to evaluate the habitability of aqueous solutions (Grant, 2004; Stevenson et al., 2015).

Despite the importance of a_w for understanding liquid water dynamics on Mars, there are few a_w datasets available for low-temperature aqueous solutions. The most detailed and accurate a_w data available for perchlorates are at 298.15 K, where a_w has been measured at concentrations ranging from dilute solutions to near saturation (e.g. Stokes and Levien, 1946; Robinson et al., 1953). At lower temperatures, a_w data is only available from freezing-point depression (FPD) measurements (e.g. Toner et al., 2015b), which extend from dilute solutions near 273.15 K to the eutectic. At temperatures and concentrations between the FPD line and 298.15 K, we are aware of no a_w measurements.

To extrapolate water activities in perchlorate solutions beyond the range of experimental data, Marion et al. (2010) and Toner et al. (2015b) fit experimental a_w data on perchlorates to the Pitzer model (Pitzer, 1991). Such models have been used to predict a_w in solutions far beyond existing experimental data points (Gough et al., 2011, 2014; Toner et al., 2015b). However, extrapolations based on Pitzer models are problematic because Pitzer models are notorious for being inaccurate beyond the range of experimental data (Rowland et al., 2015). In making revisions to the FREZCHEM Pitzer model (Marion et al., 2010), which includes perchlorate, (Toner et al., 2014b, 2015a,b) have found that inaccurate model predictions are common when models are extrapolated beyond their experimental foundations. This deficiency points to a need for more complete a_w data for perchlorates.

In this study, we determine heat capacities as a continuous function of temperature at various concentrations in aqueous $NaClO_4$, $Ca(ClO_4)_2$, and $Mg(ClO_4)_2$ solutions using Differential Scanning Calorimetry (DSC). We then use the heat capacity data, in combination with a_w and enthalpy data from literature sources at 298.15 K, to numerically calculate a_w as a function of concentration and temperature (178.15–298.15 K). As opposed to previous studies that use the Pitzer equations to calculate water activities as a function of temperature, we use smooth polynomial and spline fits to represent the available experimental data as closely as possible.

2. METHODS

2.1. DSC analysis

2.1.1. Instrument, materials, and sample preparation

We measured heat capacities using a Q2000 DSC manufactured by TA Instruments. Our DSC is cooled by liquid nitrogen and uses helium as a purge gas at a flow rate of 25 ml min^{-1}. A DSC measures the heat flux, Φ (J s^{-1} g^{-1}), in a sample relative to a reference material as the sample is heated or cooled at a constant rate, r (K s^{-1}). The specific heat capacity, C_{sp} (J K^{-1} g^{-1}), is the measured heat flux divided by the rate of temperature change ($C_{sp} = \Phi/r$). For both calibration and analysis of heat capacities, we used the same temperature protocol over all runs: (1) a 5 min isothermal period at 323 K, (2) a 10 K min^{-1} cooling scan to 173 K, and (3) a 5 min isothermal period at 173 K. We performed three separate analyses of heat capacity for each sample, and report the average heat capacity values over all three runs.

We prepared near-saturated stock solutions of $NaClO_4$, $Mg(ClO_4)_2$, and $Ca(ClO_4)_2$ using $NaClO_4{\cdot}H_2O$, $Ca(ClO_4)_2{\cdot}4H_2O$, and $Mg(ClO_4)_2{\cdot}6H_2O$ from Sigma–Aldrich®, which we further purified by recrystallizing the salts twice. These stock solutions were analyzed for concentration gravimetrically by dehydrating the salt solutions in a vacuum oven (0.02 mbar pressure) overnight at ~500 K. Replicate measurements of the stock solution concentrations gave values within ±0.01 mol kg^{-1} of each other. Solutions of known concentration were prepared by diluting the stock solutions with deionized water.

Aqueous samples were analyzed for heat capacity in Tzero™ alodined aluminum sample pans (alodine is a corrosion resistant chromate conversion coating). We pipetted 20 μL (20–30 mg) of solution into the sample pans, and then sealed the pans hermetically with an aluminum lid to prevent vapor transfer. The weight of sample pan, lid, and aqueous sample was determined before and after the DSC analysis to an accuracy of ±0.001 mg to ensure that the hermitic seal held over the course of the experiment.

2.1.2. Temperature calibration

Calibration of a DSC for heat capacity measurements requires both a temperature and heat flux calibration (Price, 1995; Höhne et al., 1996; Giuseppe et al., 2006). For the temperature calibration, we performed temperature scans through phase transition temperatures in various substances (described below) at heating rates ranging from 5 K min^{-1} to 20 K min^{-1}. We then extrapolated the onset temperature of the measured transition to a scanning rate of 0 K min^{-1} by assuming a linear dependence for the onset temperature with scanning rate. Additionally, we performed a step-scan temperature calibration, in which we increased the temperature near a transition of interest in steps of 0.05 K with 2 min isothermal intervals. Both methods of temperature calibration gave concordant results. The difference between measured (T_{meas}) and instrumental

(T_{instr}) temperatures ($\Delta T = T_{meas} - T_{instr}$) was interpolated over all temperatures by a cubic spline fit to T_{instr} vs. ΔT.

We used five different substances for temperature calibration of the DSC: 18 MΩ deionized water, 99.97% indium from TA Instruments, 99.9% cyclohexane and 99.5% cyclopentane from Crescent Chemical Co., and 99.9999% mercury from Sigma–Aldrich®. The transition temperatures we included in our calibration are the melting points of indium (429.75 K), ice (273.15 K), and mercury (234.32 K), and crystal-crystal transitions in cyclohexane (186.1 K) and cyclopentane (122.38 K). Cyclopentane has a second crystal-crystal transition temperature at 138.06 K that is recommended for DSC calibration (Höhne et al., 1996); however, we found that the temperature of this transition is subject to significant metastability during both heating and cooling, so we did not use this point in our calibration.

2.1.3. Heat flux calibration

In a heat flux calibration, the measured heat flux in a reference sample (Φ_{ref}) relative to a baseline heat flux (Φ_{base}) is compared to the actual heat flux in the reference (Φ_{real}):

$$E(T) = \frac{\Phi_{ref} - \Phi_{base}}{\Phi_{real}} \tag{1}$$

where $E(T)$ is a temperature-dependent calibration factor to be applied to subsequent measurements of the heat flux on unknown samples. For heat flux standards we used deionized water and a ~23 mg synthetic sapphire standard supplied by TA Instruments. Heat flux calibrations were performed at the beginning of an experimental run, and then periodically, in the following way: (1) we analyzed empty hermetically sealed pans on the reference and sample sensors to establish a baseline heat flux, (2) we analyzed the sapphire disc sample, with the sample pan from the previous step on the reference sensor, and (3) we analyzed a 20 μL water sample, again using the sample pan from the previous step on the reference sensor.

The use of water as a heat flux calibration material is ideal because its heat capacity and sample geometry are similar to the aqueous salt solutions we are analyzing; however, bulk water crystallizes near 250 K, and so it cannot be used at lower temperatures. We find that the calibration factor $E(T)$ for pure water is slightly lower than the calibration factor determined for sapphire by a constant amount (~2.5%) from 273 to 300 K. This is probably because the water sample is in direct contact with the sides of the sample pan, whereas the sapphire disk we use is only in contact with the bottom of the sample pan. As a result, the water sample should experience a greater rate of heat loss to the helium purge gas than the sapphire sample. To extend the calibration factor $E(T)$ measured in pure water to subzero temperatures, we assume that the sapphire and water calibration factors differ by a constant amount at all temperatures. Hence, $E(T)$ is given by:

$$E(T) = E_{\text{sapphire}}(T) - [E_{\text{sapphire}}(273\ K) - E_{\text{water}}(273\ K)] \tag{2}$$

To improve the accuracy of our experimental results, we experimented with a number of different combinations of purge gas (He or N_2), purge gas flow rates, sample mass, and DSC configurations before arriving at our current methodology. In particular, we have found that a lengthy warm up period for the DSC (2–4 h), in which the DSC is repeatedly cycled through the same temperature program to be used in later analyses, greatly improves the baseline stability. We also found that baseline shifts due to changes in room temperature and exposure to drafts could be eliminated by covering the DSC with a close-fitting box.

2.2. Thermodynamic calculations of water activity from heat capacity measurements

To calculate the temperature dependence of water activities from heat capacity data, we use the following fundamental thermodynamic relations. The change in water activity with respect to temperature (T) at constant molality and pressure is given by (Lewis et al., 1961):

$$\frac{\partial \ln a_w}{\partial T} = -\frac{\bar{L}_1}{RT^2} \tag{3}$$

where $\bar{L}_1$ (J mol^{-1}) is the relative partial molar enthalpy of water and R is the universal gas constant (8.31446 J K^{-1} mol^{-1}). $\bar{L}_1$ can be determined from apparent relative molar enthalpies of solution ($^{\phi}L$) by the equation (Lewis et al., 1961):

$$\bar{L}_1 = -\frac{m^2}{n_w}\frac{\partial^{\phi} L}{\partial m} \tag{4}$$

where n_w is the moles of water in 1 kg of water (55.5084 mol kg^{-1}) and m is molality (mol kg^{-1}). The change in $\bar{L}_1$ with temperature is given by the relative partial molar heat capacity of water, $\bar{J}_1$ (J K^{-1} mol^{-1}):

$$\bar{J}_1 = \bar{C}_{p,1} - C^0_{p,1} = \frac{\partial \bar{L}_1}{\partial T} \tag{5}$$

Here $\bar{C}_{p,1}$ is the partial molar heat capacity of water in solution and $C^0_{p,1}$ is the molar heat capacity of pure water. $\bar{C}_{p,1}$ in Eq. (5) is related to the specific heat capacity of solution, C_p (J K^{-1}), and the partial molar heat capacity with respect to solute, $\bar{C}_{p,2}$ (J K^{-1} mol^{-1}):

$$C_p = n_w\bar{C}_{p,1} + m\bar{C}_{p,2} \tag{6}$$

where C_p is calculated from measured specific heat capacities, C_{sp} (J K^{-1} g^{-1}), and the molecular weight of the solute, M_s (g mol^{-1}), by the relation:

$$C_p = C_{sp}(1000 + M_s m) \tag{7}$$

Combining Eqs. (3) and (5), and integrating with respect to a reference temperature (T_{ref}) at 298.15 K gives water activity (a_w) as a function of temperature at constant molality and pressure:

$$R\ln a_w = R\ln a_{w,T_{ref}} + \bar{L}_{1,T_{ref}}\left(\frac{1}{T} - \frac{1}{T_{ref}}\right) - \int_{T_{ref}}^{T}\left(\frac{1}{T^2}\int_{T_{ref}}^{T}(\bar{C}_{p,1} - C^0_{p,1})dT\right)dT \tag{8}$$

To evaluate $\bar{C}_{p,1}$ in this equation, we (1) fit measured C_p values determined in this study using a smooth function (described below in Section 2.2.3), (2) calculate $\bar{C}_{p,2}$ as

$\partial C_p/\partial m$, and (3) calculate $\bar{C}_{p,1}$ using Eq. (6). We then evaluate Eq. (8) by numerically integrating $\bar{C}_{p,1}$ with temperature, using literature data for the values of $C^0_{p,1}$, $a_{w,T_{ref}}$, and $\bar{L}_{1,T_{ref}}$.

2.2.1. Heat capacity of pure water ($C^0_{p,1}$)

For $C^0_{p,1}$, we use values given in Clegg and Brimblecombe (1995) and Murphy and Koop (2005) (Fig. 1). Clegg and Brimblecombe (1995) extrapolated $C^0_{p,1}$ into the supercooled region by assuming a constant value for $\partial^2 C^0_{p,1}/\partial T^2$ below 273.15 K and integrating to determine $C^0_{p,1}$ at lower temperatures using 273.15 K as a reference temperature. This heat capacity extrapolation forms the basis for low-temperature water activities in the widely-used aqueous planetary model FREZCHEM (Marion and Kargel, 2008). Murphy and Koop (2005) review a number of different extrapolations of $C^0_{p,1}$ in supercooled water. Their nominal $C^0_{p,1}$ curve is based on the $C^0_{p,1}$ measurements of Archer and Carter (2000) above 236 K, and is extrapolated to lower temperatures by considering several thermodynamic constraints (see discussion in Murphy and Koop, 2005). The $C^0_{p,1}$ curve in Murphy and Koop (2005) is in much better agreement with heat capacity measurements on supercooled water from Archer and Carter (2000). Furthermore, the shape of the curve at even lower temperatures is consistent with current theoretical and experimental studies suggesting that $C^0_{p,1}$ reaches a maximum value at a liquid–liquid critical point near 225 K (Holten et al., 2012).

2.2.2. Water activity and relative partial molar enthalpy of water at 298.15 K

To calculate the activity of water at 298.15 K, we smooth experimentally determined water activities from literature sources (Table 1) with cubic splines and interpolate a_w at different concentrations. Similarly, to calculate the partial molar enthalpy of water at 298.15 K, we fit experimentally determined apparent molar enthalpies of solution ($^{\phi}L$) from literature sources at 298.15 K using cubic splines. We then interpolate $\partial^{\phi}L/\partial m$ using the fitted spline, and calculate $\bar{L}_1$ using Eq. (4). Our rationale for using spline fits, as opposed to existing Pitzer model parameters for water activity and enthalpy (e.g. Toner et al., 2015b), is because the Pitzer model often deviates significantly from experimental data at high concentrations. By using cubic splines, we avoid such misfits, and our interpolated values represent the experimental data as closely as possible.

With the exception of $^{\phi}L$ in $Mg(ClO_4)_2$ solutions and a_w in $Ca(ClO_4)_2$ solutions, $^{\phi}L$ and a_w have been determined in $NaClO_4$, $Ca(ClO_4)_2$, and $Mg(ClO_4)_2$ solutions within the range of concentrations measured in this study. In $Mg(ClO_4)_2$ solutions, $^{\phi}L$ has been measured up to 3.2 molal. To extrapolate our calculated $\bar{L}_1$ values in $Mg(ClO_4)_2$ solutions to the maximum molality of 4.25 investigated in this study, we fit our $\bar{L}_1$ values from 2.5 to 3.2 molal to a quadratic equation and extrapolate this equation to 4.25 molal. Our rationale for this methodology is based on the quadratic shape of interpolated $\bar{L}_1$ values as a function of molality in concentrated $Ca(ClO_4)_2$ solutions, and the similar concentration dependence of $\bar{L}_1$ in $Ca(ClO_4)$ and $Mg(ClO_4)_2$ solutions (see Section 3.2). In $Ca(ClO_4)_2$ solutions, a_w has been measured up to 6.9 molal. To extrapolate these measurements to the maximum molality of 7.57 investigated in this study, we assume a linear concentration dependence in $\ln a_w$ above 6.9 molal, noting that $\ln a_w$ becomes nearly linear at high concentrations.

2.2.3. Partial molar heat capacities

To smooth experimentally determined specific heats of solution for calculation of the partial molar heat capacities of solution, we fit our experimental heat capacity measurements to the following empirical equation:

$$C_p(m,T) = \sum_{j=0}^{j=4}\sum_{i=0}^{i=3} P_{ij} m^j T^i \quad (9)$$

where P_{ij} are empirical coefficients (Table 2). Using Eq. (9), we calculate the partial molar heat capacity with respect to water ($\bar{C}_{p,1}$) via Eq. (6).

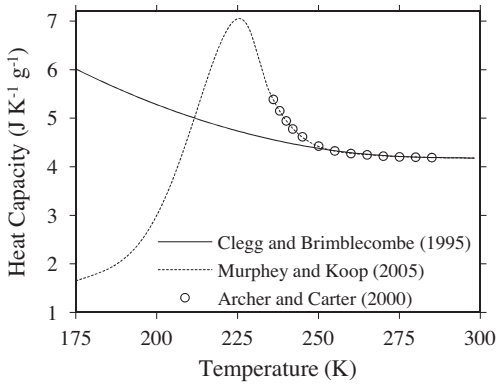

Fig. 1. Extrapolations of the heat capacity of water ($C^0_{p,1}$) into the supercooled region from Clegg and Brimblecombe (1995) and Murphy and Koop (2005). Experimental heat capacity measurements on supercooled water from Archer and Carter (2000) are given by the circles.

3. RESULTS

3.1. Heat capacity as a function of temperature and composition

Specific heat capacities measured in $NaClO_4$, $Ca(ClO_4)_2$, and $Mg(ClO_4)_2$ solutions decrease with temperature at all concentrations (Figs. 2; S1; Tables A1–A3). None of the solutions we measured showed increases in specific heat capacity at low concentrations, as has been found by Archer and Carter (2000) in NaCl and Carter and Archer (2000) in $NaNO_3$ solutions. This is because these studies measured heat capacities in aqueous emulsions, allowing for deep supercooling in relatively dilute solutions. In contrast, our measurements were done on bulk solutions, so that ice and/or salt crystallized before the temperature could decrease to the point where the heat capacity might increase. At concentrations below the eutectic concentration

Table 1
Sources of literature water activity (a_w) and solution enthalpy ($^{\phi}L$) data at 298.15 K used in this study. The maximum concentration of experimental measurements is given in mol kg^{-1} to the right of the references.

	Water activity		Solution enthalpy	
Salt	Source	Molality (mol kg^{-1})	Source	Molality (mol kg^{-1})
$NaClO_4$	Jones (1947)	6.4	Vanderzee and Swanson (1963)	17.1
	Miller and Sheridan (1956)	16.2		
	Rush and Johnson (1968)	17.9		
	Rush and Johnson (1971)	16.0		
	Rush (1988)	14.9		
$Ca(ClO_4)_2$	Robinson et al. (1953)	6.9	Gier and Vanderzee (1974)	7.7
$Mg(ClO_4)_2$	Stokes and Levien (1946)	4.4	Jongenburger and Wood (1965)	3.2

Table 2
Empirical parameters P_{ij} derived by fitting our experimental heat capacity data to Eq. (9).

ij	$NaClO_4$	$Ca(ClO_4)_2$	$Mg(ClO_4)_2$
00	3.4771E−01	1.3777E+00	2.5571E+00
01	2.6491E−02	5.8219E−03	3.5174E−03
02	−4.1015E−05	5.8731E−05	4.4696E−05
03	−4.5871E−09	−1.5273E−07	−1.3583E−07
10	−2.9450E−01	5.9276E−01	−1.1101E+00
11	−1.7092E−03	−1.8327E−03	1.6726E−03
12	3.1590E−06	−6.5756E−06	1.2114E−05
13	−1.3510E−08	6.9490E−09	−5.0080E−09
20	−3.6119E−01	−1.6762E−01	3.6474E−01
21	4.1701E−03	9.6063E−04	−3.2900E−03
22	−8.8064E−07	5.0638E−06	5.6849E−06
23	1.1722E−09	−8.5719E−09	−3.8006E−09
30	1.0897E−01	−2.5809E−02	2.8468E−01
31	−1.2083E−03	9.0345E−05	7.2784E−04
32	−4.4554E−07	9.1830E−08	−5.7020E−06
33	1.2143E−09	−1.8717E−09	4.0534E−09
40	8.4745E−02	5.4041E−03	−3.5080E−02
41	−3.2037E−04	2.2588E−05	−1.4751E−04
42	2.2572E−07	−3.4117E−07	6.7041E−07
43	9.4339E−10	8.1064E−10	7.6620E−10

of the solutions (9.23 m $NaClO_4$, 4.17 m $Ca(ClO_4)_2$, and 3.38 m $Mg(ClO_4)_2$), we were able to supercool our solutions with respect to ice by 20–30 K. Near the eutectic concentration, the solutions were easily supercooled to 173 K. Above the eutectic concentration, supercooling was limited by precipitation of salt phases.

We evaluate the error in our heat capacity measurements by comparing between the three replicate heat capacity measurements, and to literature data when available. The standard deviation of the mean between the three replicate measurements of heat capacity is always less than ±0.3% at all temperatures. This consistency between replicate measurements indicates that our calibration and analysis procedure reduces the instrumental error to about as low as can be expected for DSC analyses (Archer and Carter, 2000).

Apart from this study, there are few experimental studies on the heat capacity of concentrated perchlorate solutions that we can compare our results to. The heat capacity of aqueous $NaClO_4$ has been measured up to 16.7 molal at 298.15 K using a flow calorimeter by Roux et al. (1978). Our heat capacities are within ±0.7% of Roux et al. (1978) on average, although the difference is

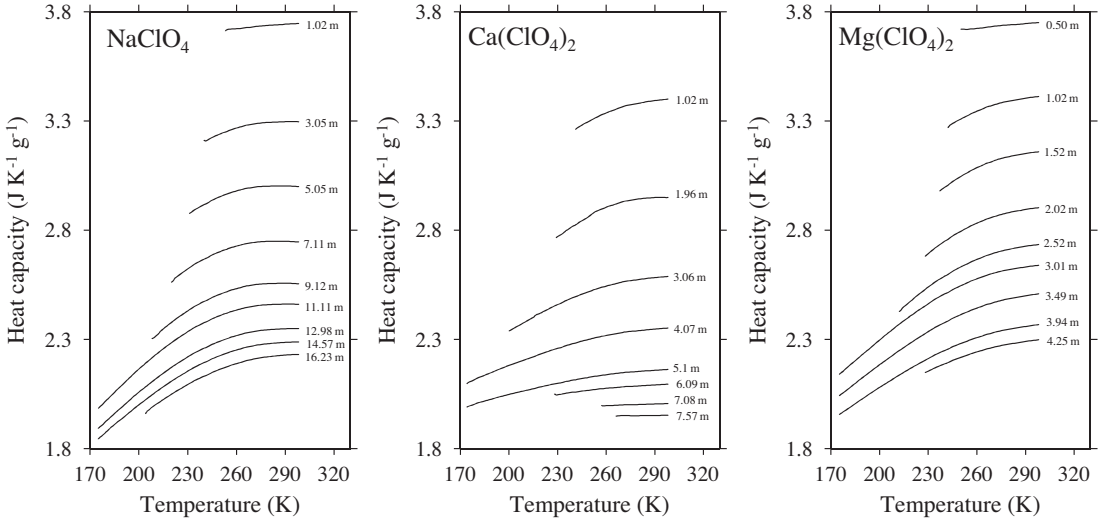

Fig. 2. Specific heat capacities (C_{sp}) in $NaClO_4$, $Ca(ClO_4)_2$, and $Mg(ClO_4)_2$ solutions measured at various concentrations as a function of temperature during cooling scans (10 K min^{-1}). The DSC measures heat capacity as a continuous function of temperature, so heat capacities are shown as curves.

as high as 2% for the 5.52 molal $NaClO_4$ sample (Fig. 3). Heat capacities in $Ca(ClO_4)_2$ and $Mg(ClO_4)_2$ solutions have been measured at 298.15 K by Latysheva and Andreeva (1975) up to 4 molal concentration. Comparisons between our results and Latysheva and Andreeva (1975) at similar concentrations indicate close agreement in heat capacities, with the exception of 2 molal $Mg(ClO_4)_2$ solutions, where the difference in heat capacity is 2% (Fig. 3). These larger errors indicate that there are additional systematic errors in our DSC analysis, probably due to slight differences in sample pan geometry, sample heat conductivity, and contact geometry with the DSC sensors. Taking into account both instrumental and systematic errors, we estimate that our heat capacity measurements are accurate to 1–2%, which can be compared with typical accuracies attainable with DSC instruments of 5–15% (Höhne et al., 1996). Eq. (9) is able to fit our experimental heat capacities to within our estimated experimental errors of 1–2% (Table 2).

3.2. Interpolated water activities and enthalpies

Experimental water activities and apparent relative molar enthalpies at 298.15 K are well represented by both spline fits (this study) and the Pitzer model of Toner et al. (2015b), although at high concentrations the Pitzer model predictions for $NaClO_4$ and $Ca(ClO_4)_2$ show slight deviations from experimental measurements (Fig. 4A and B). With respect to ${}^{\phi}L$, relatively small errors in Pitzer model predictions become much more significant when the partial molar enthalpy of water ($\bar{L}_1$) is calculated via Eq. (4), as shown in Fig. 4C. In the case of $NaClO_4$, the Pitzer equations even predict the opposite sign for $\bar{L}_1$ at high concentrations, which has a large effect on calculated water activities at low temperatures, as discussed in the following section (Section 3.3). The Pitzer model used in Toner et al. (2015b) assumes that electrolytes in solution are fully dissociated i.e. ion pairing is not explicitly included in the model. As discussed below in Section 4, there is significant evidence that ion pairing is stronger at low temperatures, which suggests that better model fits could be obtained by explicitly including ion pairs in the Pitzer model. Regardless, the differences between spline fits to experimental data and Pitzer model fits of Toner et al. (2015b) suggests that one should be cautious about Pitzer model predictions at high concentrations, particularly when calculating partial molar properties from the Pitzer equations.

3.3. Water activity as a function of temperature and composition

Water activities in $NaClO_4$ solutions calculated using Eq. (8) increase with decreasing temperature at all concentrations, by as much as 0.25 a_w from 298.15 K to 175 K in concentrated solutions (Fig. 5). In contrast, water activities in $Ca(ClO_4)_2$ and $Mg(ClO_4)_2$ solutions decrease with decreasing temperature above ~200 K, and then increase below about 210 K. Above ~230 K, water activities calculated using the $C^0_{p,1}$ curves in Clegg and Brimblecombe (1995) and Murphy and Koop (2005) are similar; whereas, below ~230 K, water activities calculated using the curve in Murphy and Koop (2005) are higher by about 0.05 a_w on average.

Compared to the low-temperature Pitzer model in Toner et al. (2015b), the water activities we calculate in concentrated, low-temperature $NaClO_4$ solutions are much higher than Pitzer model predictions, by as much as 0.3 a_w at 175 K. This can be attributed to the different sign in $\bar{L}_1$ at 298.15 K at high concentrations predicted by the Pitzer model (see Fig. 4C). The differences between our a_w calculations and the Pitzer model of Toner et al. (2015b) are much less striking in $Ca(ClO_4)_2$ and $Mg(ClO_4)_2$ solutions, although significant differences occur between 175 and 220 K. In concentrated $NaClO_4$ and $Ca(ClO_4)_2$ solutions at 298.15 K, the Pitzer model of Toner et al. (2015b) also underestimates a_w. Pitzer model parameters at 298.15 K in Toner et al. (2015b) are taken from Pitzer (1991). In determining Pitzer parameters, Pitzer (1991) gave less weight to all data above an ionic strength of 4 molal by assigning a reduced weight to this data of $(4/I)^2$, where I is the ionic strength. Furthermore, experimental data above $I = 6$ mol kg^{-1} were not used in model fits. This bias towards low concentrations explains the poorer fit to experimental a_w data in near-saturated solutions. Overall, water activities in the model of Toner et al. (2015b) are similar to our calculated water activities in equilibrium solutions, particularly at sub-eutectic concentrations, but can differ markedly in supercooled/supersaturated solutions.

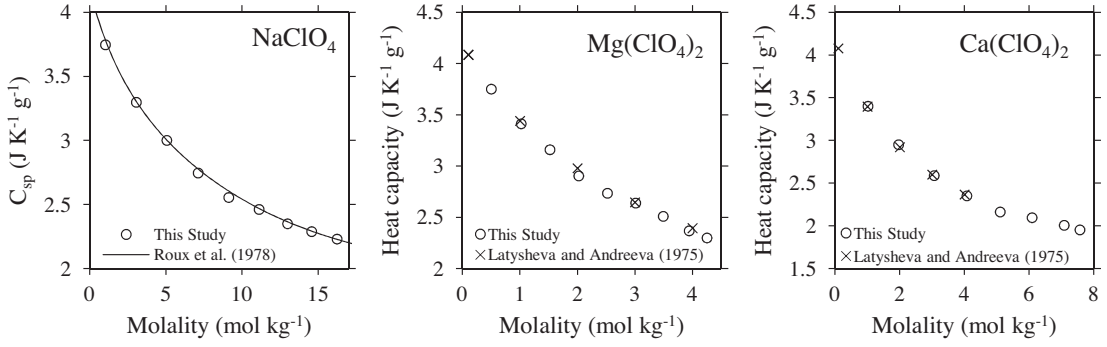

Fig. 3. Specific heat capacities (C_{sp}) in $NaClO_4$, $Ca(ClO_4)_2$, and $Mg(ClO_4)_2$ solutions measured at 298.15 K as a function of concentration (mol kg^{-1}) from this study and from literature sources.

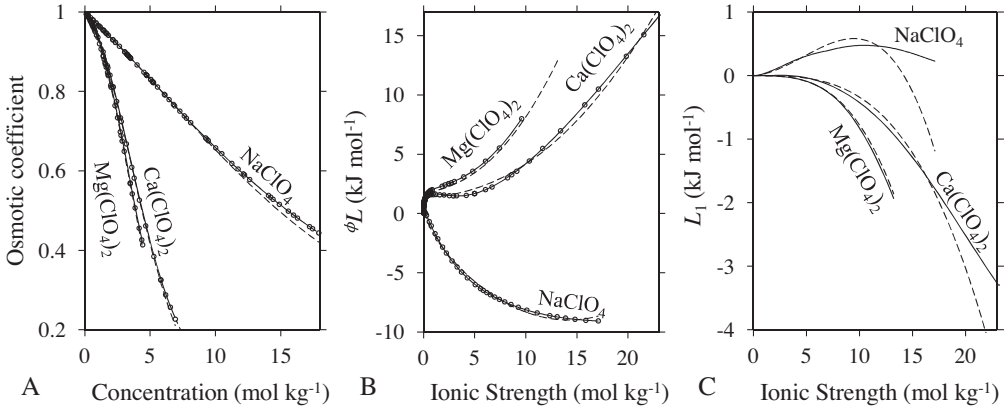

Fig. 4. Osmotic coefficients (A), apparent relative molar enthalpy ($^{\phi}L$) (B), and relative molar enthalpy of water ($\bar{L}_1$) (C) in $NaClO_4$, $Ca(ClO_4)_2$, and $Mg(ClO_4)_2$ solutions at 298.15 K. Circles (o) indicate experimental data points from the literature sources in Table 1. Solid lines (—) are interpolated values using cubic-spline fits. Dashed lines (----) are derived from the low-temperature thermodynamic model of Toner et al. (2015b). Ionic strength for 1–1 electrolytes like $NaClO_4$ is equal to the molality, whereas for 2-1 electrolytes like $Mg(ClO_4)_2$ the ionic strength is equal to three times the molality.

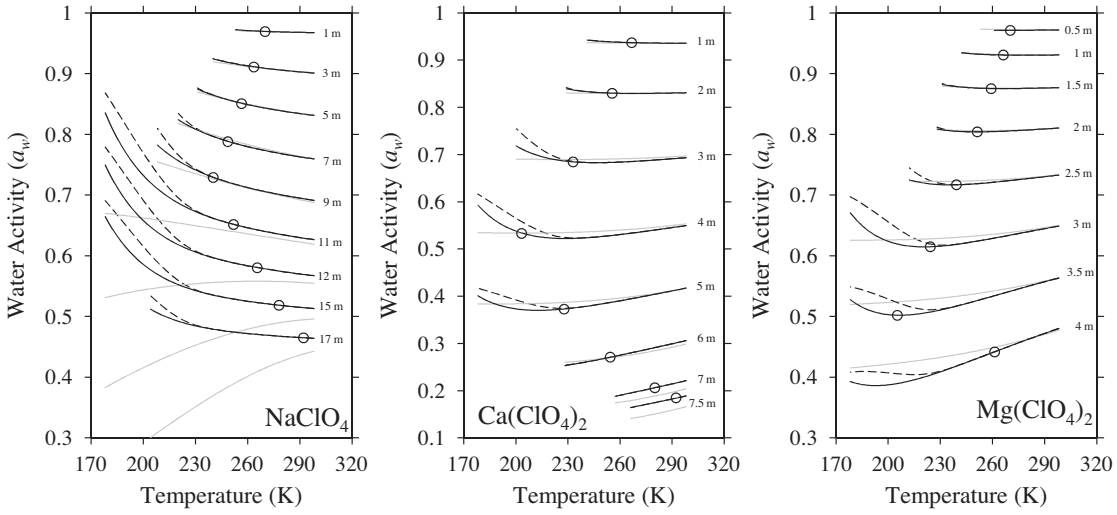

Fig. 5. Water activities as a function of temperature and concentration calculated using Eq. (8) for $NaClO_4$, $Ca(ClO_4)_2$, and $Mg(ClO_4)_2$ brines. The solid lines (——) are calculated using $\bar{C}^0_{p,1}$ from Clegg and Brimblecombe (1995), the dashed lines (-----) using $\bar{C}^0_{p,1}$ from Murphy and Koop (2005), and the gray solid lines (——) are calculated from the low-temperature Pitzer model of Toner et al. (2015b). The circles indicate the point at which ice or salt would precipitate out of solution at equilibrium conditions.

To evaluate the accuracy of our water activity calculations, we compare our results to water activities determined from freezing-point depression measurements in Toner et al. (2015b) (Fig. 6). For $NaClO_4$ and $Ca(ClO_4)_2$, the agreement between the two water activity measurements is excellent, down to 200 K in the case of $Ca(ClO_4)_2$. For $Mg(ClO_4)_2$, water activities calculated in this study are in close agreement with freezing-point depression values at higher temperatures, but at the lowest freezing-point depression of 3 molal and 225 K, the two methods differ by 0.01 a_w. Possibly, this error is due to uncertainty in the value of $\bar{L}_1$, which is based on only a few enthalpy measurements near 3 molal concentration and is extrapolated to higher concentrations (see Fig. 4B).

4. DISCUSSION

The temperature dependence of water activity in salt solutions is a function of both the relative partial molar enthalpy ($\bar{L}_1$) and heat capacity ($\bar{J}_1$) of water; however, in the following discussion, we show that it is primarily the sign of $\bar{L}_1$ at 298.15 K that determines the overall shape of the water activity curve with temperature in perchlorate solutions. Eq. (5) indicates that the change in $\bar{L}_1$ with temperature is given by $\bar{J}_1$: if $\bar{J}_1 < 0$ then $\bar{L}_1$ increases when temperature decreases. We find that $\bar{J}_1$ is negative (meaning that $\bar{C}_{p,1}$ is less than $C^0_{p,1}$) at all concentrations and temperatures investigated in this study (see Figs. S2 and S3 in the supplementary material for graphs of partial molar heat

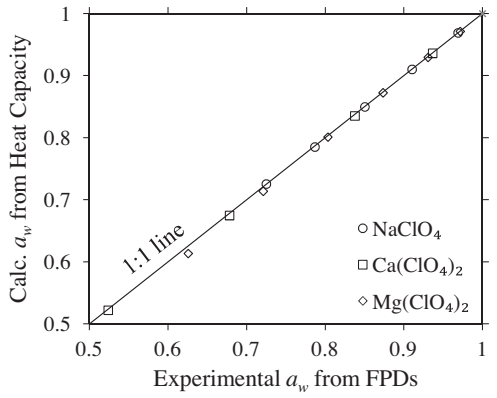

Fig. 6. A comparison between water activities determined from experimental freezing-point depressions from Toner et al. (2015b), and water activities calculated at the freezing point using heat capacities in this study. Note: water activities determined from freezing-point depressions in Toner et al. (2015b) are based on the pure water heat capacity ($\bar{C}^0_{p,1}$) curve in Clegg and Brimblecombe (1995).

capacities). A negative value for $\bar{J}_1$ is consistent with the physical interpretation that aqueous electrolytes lower the heat capacity of pure water by (1) breaking the hydrogen bonded network of water and (2) lowering the degrees of freedom of water by binding water into hydration spheres around charged ions (Randall and Rossini, 1929). Furthermore, negative value for $\bar{J}_1$ indicates that $\bar{L}_1$ always increases with decreasing temperature.

Eq. (3) indicates that $\bar{L}_1$ is inversely proportional to the change in ln a_w with temperature. In $NaClO_4$ solutions, $\bar{L}_1$ is already positive at 298.15 K, and as a result, water activities only increase with decreasing temperature. In contrast, $\bar{L}_1$ is negative at 298.15 K in $Mg(ClO_4)_2$ and $Ca(ClO_4)_2$ solutions, but becomes positive near 200–230 K. This leads to a "U" shaped water activity curve; water activity initially decreases with decreasing temperature, and then increases once $\bar{L}_1$ becomes positive. Hence, the value of $\bar{L}_1$ at 298.15 K can be used to qualitatively evaluate whether water activities will monotonically increase with decreasing temperature, as in $NaClO_4$ solutions, or exhibit a "U" shaped temperature dependence, as in $Mg(ClO_4)_2$ and $Ca(ClO_4)_2$ solutions.

Water activity trends in this study can be compared to the decrease in ion activity coefficients with decreasing temperature modeled in NaCl and $NaNO_3$ solutions below 273.15 K (Archer and Carter, 2000; Carter and Archer, 2000). Decreasing ion activity coefficients in these solutions have been attributed to increased ion pair formation at low temperatures (see discussion in Carter and Archer (2000) on ion pairing). An increase in ion pair formation implies a corresponding increase in water activity because the additional ion-ion interactions would disrupt ion–solvent interactions, freeing up water in the solution. The increase in water activity in $NaClO_4$ solutions with decreasing temperature is consistent with this interpretation; however, the increase in water activity in $Mg(ClO_4)_2$ and $Ca(ClO_4)_2$ solutions only occurs at low temperatures, around 200–220 K. We suggest that the onset of ion-association effects in $Mg(ClO_4)_2$ and $Ca(ClO_4)_2$ solutions may be delayed because water molecules are more tightly bound in hydration spheres due to the higher cation charge, making it more difficult for ion association to occur compared to $NaClO_4$ solutions.

The ion association effects discussed above are consistent with values for $\bar{L}_1$ in perchlorate solutions. Experimentally, $\bar{L}_1$ is given by the enthalpy due to the addition of a small quantity of pure water to a large quantity of salt solution (Lewis et al., 1961), and its value is determined by endothermic breaking of the hydrogen bonding network of pure water vs. exothermic formation of ion-water interactions. A positive value for $\bar{L}_1$ in $NaClO_4$ solutions suggests that endothermic breaking of hydrogen bonds predominates, which implies relatively weak ion-water interactions. In contrast, a negative value for $\bar{L}_1$ at 298.15 K in $Mg(ClO_4)_2$ and $Ca(ClO_4)_2$ solutions suggests strong exothermic ion-water interactions due to the higher cation charge.

What do our results imply about the formation and habitability of perchlorate brines on Mars? The increase in $NaClO_4$ water activities suggests that, at least in terms of water activity, $NaClO_4$ brines are more habitable at lower temperatures; in contrast, $Mg(ClO_4)_2$ and $Ca(ClO_4)_2$ brines generally become less habitable at lower temperatures. In deeply supercooled brines, water activity increases with decreasing temperature, remarkably so in $NaClO_4$ solutions. Toner et al. (2014a) found that perchlorate salts can easily supercool down to their glass transition at ~150 K, even at slow cooling rates of 0.2 K min^{-1} (relevant to diurnal rates of temperature change on Mars in the summer) and in the presence of soil particles. Such glasses could preserve organics from the damaging effects of ice or salt crystallization, and are a potential mechanism for life to survive the extreme drops in temperature that occur during Martian nights and winters. The water activity data in this study indicate that water activity in such supercooled solutions is either similar to, or greatly increases above, water activities at 298.15 K.

Water activity changes also affect the formation of liquid water. The increase in $NaClO_4$ water activity indicates that these solutions will become less hygroscopic at lower temperatures i.e. more prone to evaporation; in contrast, $Mg(ClO_4)_2$ and $Ca(ClO_4)_2$ solutions will become slightly more hygroscopic. Furthermore, an increase in water activity with decreasing temperature indicates that the freezing point of ice will occur at higher temperatures than if water activities remained constant with temperature. For example, if the water activity in a 9 molal solution of $NaClO_4$ did not change from its value at 298.15 K, then ice would freeze from solution at 235.2 K instead of at the experimental temperature of 240.6 K.

5. CONCLUSIONS

Water activity is fundamental towards understanding the potential habitability of aqueous solutions and the formation of liquid water on Mars; however, there is a critical lack of water activity data in perchlorate solutions below

298.15 K and at concentrations above the ice equilibrium line. In this study, we derive water activities in variable concentration $NaClO_4$, $Mg(ClO_4)_2$, and $Ca(ClO_4)_2$ solutions from 298.15 to 178.15 K using experimental heat capacity measurements. Our results indicate that water activities in $NaClO_4$ solutions strongly increase with decreasing temperature, by as much as 0.25 a_w from 298.15 to 178 K. In contrast, $Mg(ClO_4)_2$ and $Ca(ClO_4)_2$ solutions have a "U" shaped a_w curve, first decreasing with decreasing temperature, and then increasing below 220 K. These effects can

Table A1
Average specific heat capacities (C_{sp}, J K^{-1} mol^{-1}) of three replicate measurements in different concentration (mol kg^{-1}) $NaClO_4$ solutions as a function of temperature (K). Values are given at 10 K intervals.

Temp. (K)	1.02 m	3.05 m	5.05 m	7.11 m	9.12 m	11.11 m	12.98 m	14.57 m	16.23 m
298.15	3.746	3.297	3.000	2.746	2.555	2.461	2.350	2.289	2.230
288.15	3.742	3.297	3.003	2.748	2.557	2.462	2.349	2.286	2.227
278.15	3.737	3.293	3.002	2.748	2.555	2.459	2.344	2.280	2.219
268.15	3.729	3.283	2.994	2.740	2.547	2.449	2.333	2.267	2.205
258.15	3.722	3.264	2.976	2.723	2.529	2.431	2.314	2.248	2.185
248.15	–	3.232	2.945	2.693	2.499	2.402	2.284	2.218	2.155
238.15	–	–	2.906	2.656	2.463	2.366	2.249	2.184	2.121
228.15	–	–	–	2.607	2.416	2.321	2.206	2.142	2.080
218.15	–	–	–	–	2.362	2.269	2.156	2.094	2.035
208.15	–	–	–	–	–	2.210	2.100	2.041	1.984
198.15	–	–	–	–	–	2.145	2.041	1.984	–
188.15	–	–	–	–	–	2.073	1.974	1.923	–
178.15	–	–	–	–	–	1.998	1.905	1.858	–

Table A2
Average specific heat capacities (C_{sp}, J K^{-1} mol^{-1}) of three replicate measurements in different concentration (mol kg^{-1}) $Ca(ClO_4)_2$ solutions as a function of temperature (K). Values are given at 10 K intervals.

Temp. (K)	1.02 m	1.96 m	3.06 m	4.07 m	5.1 m	6.09 m	7.08 m	7.57 m
298.15	3.401	2.950	2.588	2.352	2.163	2.096	2.006	1.953
288.15	3.392	2.949	2.581	2.346	2.157	2.091	2.003	1.952
278.15	3.379	2.941	2.572	2.338	2.152	2.086	2.001	1.951
268.15	3.360	2.926	2.559	2.329	2.146	2.082	1.999	1.951
258.15	3.331	2.900	2.540	2.315	2.136	2.075	1.996	–
248.15	3.291	2.853	2.513	2.296	2.123	2.066	–	–
238.15	–	2.807	2.484	2.275	2.110	2.056	–	–
228.15	–	–	2.450	2.252	2.095	–	–	–
218.15	–	–	2.415	2.226	2.078	–	–	–
208.15	–	–	2.368	2.200	2.061	–	–	–
198.15	–	–	–	2.173	2.043	–	–	–
188.15	–	–	–	2.142	2.022	–	–	–
178.15	–	–	–	2.110	1.999	–	–	–

Table A3
Average specific heat capacities (C_{sp}, J K^{-1} mol^{-1}) of three replicate measurements in different concentration (mol kg^{-1}) $Mg(ClO_4)_2$ solutions as a function of temperature (K). Values are given at 10 K intervals.

Temp. (K)	0.50 m	1.02 m	1.52 m	2.02 m	2.52 m	3.01 m	3.49 m	3.94 m	4.25 m
298.15	3.751	3.412	3.159	2.903	2.735	2.639	2.509	2.368	2.299
288.15	3.744	3.402	3.148	2.892	2.724	2.629	2.497	2.357	2.289
278.15	3.739	3.388	3.134	2.878	2.710	2.617	2.484	2.344	2.277
268.15	3.731	3.368	3.111	2.856	2.689	2.598	2.464	2.326	2.260
258.15	3.722	3.339	3.080	2.826	2.660	2.572	2.439	2.303	2.239
248.15	–	3.298	3.033	2.783	2.621	2.536	2.404	2.273	2.210
238.15	–	–	2.980	2.734	2.576	2.496	2.367	2.239	2.179
228.15	–	–	–	–	2.523	2.449	2.323	2.200	–
218.15	–	–	–	–	2.463	2.397	2.275	2.159	–
208.15	–	–	–	–	–	2.340	2.223	2.113	–
198.15	–	–	–	–	–	2.280	2.169	2.067	–
188.15	–	–	–	–	–	2.217	2.113	2.017	–
178.15	–	–	–	–	–	2.152	2.054	1.966	–

be qualitatively predicted, without resorting to extensive heat capacity measurements, from the value of the partial molar enthalpy of water ($\bar{L}_1$) at 298.15 K; a positive value for $\bar{L}_1$ indicates that a_w will increase with decreasing temperature and a negative value for $\bar{L}_1$ indicates a "U" shaped a_w curve. These results imply that $NaClO_4$ solutions will become more habitable, at least in terms of water activity, at lower temperatures, whereas $Mg(ClO_4)_2$ and $Ca(ClO_4)_2$ solutions generally become less habitable at lower temperatures.

ACKNOWLEDGEMENTS

Funding from a NASA Astrobiology Institute Postdoc awarded to JDT and a NASA Habitable Worlds grant (14-HW14_2-0024).

APPENDIX A

See Tables A1–A3.

APPENDIX B. SUPPLEMENTARY DATA

Supplementary data associated with this article can be found, in the online version, at http://dx.doi.org/10.1016/j.gca.2016.03.005.

REFERENCES

Archer D. G. and Carter R. W. (2000) Thermodynamic properties of the NaCl + H_2O system. 4. Heat capacities of H_2O and NaCl (aq) in cold-stable and supercooled states. *J. Phys. Chem.* **104**, 8563–8584.

Carter R. W. and Archer D. G. (2000) Heat capacity of $NaNO_3$(aq) in stable and supercooled states. Ion association in the supercooled solution. *Phys. Chem. Chem. Phys.* **2**, 5138–5145.

Chevrier V. F. and Rivera-Valentin E. G. (2012) Formation of recurring slope lineae by liquid brines on present-day Mars. *Geophys. Res. Lett.* **39**, 1–5.

Chevrier V., Hanley J. and Altheide T. S. (2009) Stability of perchlorate hydrates and their liquid solutions at the Phoenix landing site, Mars. *Geophys. Res. Lett.* **36**, 1–6.

Clegg S. L. and Brimblecombe P. (1995) Application of a multicomponent thermodynamic model to activities and thermal properties of 0–40 mol kg^{-1} aqueous sulfuric acid from 200 to 328 K. *J. Chem. Eng. Data* **40**, 43–64.

Coates J. D. and Achenbach L. A. (2004) Microbial perchlorate reduction: rocket-fuelled metabolism. *Nat. Rev. Microbiol.* **2**, 569–580.

Davila A. F., Duport L. G., Melchiorri R., Jänchen J., Valea S., Rios A., Fairén A. G., Möhlmann D., McKay C. P., Ascaso C. and Wierzchos J. (2010) Hygroscopic salts and the potential for life on Mars. *Astrobiology* **10**, 617–628.

Fisher D. A., Hecht M. H., Kounaves S. P. and Catling D. C. (2010) A perchlorate brine lubricated deformable bed facilitating flow of the north polar cap of Mars: possible mechanism for water table recharging. *J. Geophys. Res.* **115**, E00E12.

Gier L. J. and Vanderzee C. E. (1974) Enthalpies of dilution and relative apparent molar enthalpies of aqueous calcium and manganous perchlorates. *J. Chem. Eng. Data* **19**, 323–325.

Giuseppe D. G., Della Gatta G., Richardson M. J., Sarge S. M. and Stølen S. (2006) Standards, calibration, and guidelines in microcalorimetry. Part 2. Calibration standards for differential scanning calorimetry. *Pure Appl. Chem.* **78**, 1455–1476.

Gough R. V., Chevrier V. F., Baustian K. J., Wise M. E. and Tolbert M. A. (2011) Laboratory studies of perchlorate phase transitions: support for metastable aqueous perchlorate solutions on Mars. *Earth Planet. Sci. Lett.* **312**, 371–377.

Gough R. V., Chevrier V. F. and Tolbert M. A. (2014) Formation of aqueous solutions on Mars via deliquescence of chloride–perchlorate binary mixtures. *Earth Planet. Sci. Lett.* **393**, 73–82.

Grant W. D. (2004) Life at low water activity. *Philos. Trans. Royal Soc. Lond.: Biol. Sci.* **359**, 1249–1267.

Hecht M. H., Kounaves S. P., Quinn R. C., West S. J., Young M. M., Ming D. W., Catling D. C., Clark B. C., Boynton W. V., Hoffman J., DeFlores L. P., Gospodinova K., Kapit J. and Smith P. H. (2009) Detection of perchlorate and the soluble chemistry of martian soil at the Phoenix Lander site. *Science* **325**, 64–67.

Höhne G., Hemminger W. and Flammersheim H.-J. (1996) *Differential Scanning Calorimetry: An Introduction for Practitioners*. Springer-Verlag, Berlin, New York.

Holten V., Bertrand C. E., Anisimov M. A. and Sengers J. V. (2012) Thermodynamics of supercooled water 136. *J. Chem. Phys.*

Jones J. H. (1947) Isotonic solutions: osmotic and activity coefficients of lithium and sodium perchlorates at 25 °C. *J. Phys. Chem.* **51**, 516–521.

Jongenburger H. S. and Wood R. H. (1965) The heats and entropies of dilution of the perchlorates of magnesium and strontium. *J. Phys. Chem.* **69**, 4231–4238.

Latysheva V. A. and Andreeva I. N. (1975) Study of capacity of aqueous perchlorates of 2nd group elements of periodic table. *Vestnik Leningradskogo Universiteta Seriya Fizika Khimiya*, 63–66.

Lenferink H. J., Durham W. B., Stern L. A. and Pathare A. V. (2013) Weakening of ice by magnesium perchlorate hydrate. *Mars Polar Sci. V* **225**, 940–948.

Lewis G. N., Randall M., Pitzer K. S. and Brewer L. (1961) *Thermodynamics*, second ed. McGraw-Hill.

Marion G. M. and Kargel J. S. (2008) *Cold aqueous planetary geochemistry with FREZCHEM: from modeling to the search for life at the limits*. Springer, Berlin/Heidelberg.

Marion G. M., Catling D. C., Zahnle K. J. and Claire M. W. (2010) Modeling aqueous perchlorate chemistries with applications to Mars. *Icarus* **207**, 675–685.

Miller M. L. and Sheridan C. L. (1956) Concentrated salt solutions. I. Activity coefficients of sodium thiocyanate, sodium iodide and sodium perchlorate at 25°. *J. Phys. Chem.* **60**, 184–186.

Murphy D. M. and Koop T. (2005) Review of the vapour pressures of ice and supercooled water for atmospheric applications. *Q. J. Roy. Meteorol. Soc.* **131**, 1539–1565.

Ojha L., Wilhelm M. B., Murchie S. L., McEwen A. S., Wray J. J., Hanley J., Massé M. and Chojnacki M. (2015) Spectral evidence for hydrated salts in recurring slope lineae on Mars. *Nat. Geosci.* **8**, 829–832.

Pitzer K. S. (1991) *Ion Interaction Approach: Theory and Data Correlation, Activity Coefficients in Electrolyte Solutions*, second ed. CRC Press, Boca Raton, pp. 75–153.

Price D. M. (1995) Temperature calibration of differential scanning calorimeters. *J. Therm. Anal. Calorim.* **45**, 1285–1296.

Randall M. and Rossini F. D. (1929) Heat capacities in aqueous salt solutions. *J. Am. Chem. Soc.* **51**, 323–345.

Robinson R. A., Lim C. K. and Ang K. P. (1953) The osmotic and activity coefficients of calcium, strontium and barium perchlorate at 25°. *J. Am. Chem. Soc.* **75**, 5130–5130.

Roux A., Musbally G. M., Perron G., Desnoyers J. E., Singh P. P., Woolley E. M. and Hepler L. G. (1978) Apparent molal heat

capacities and volumes of aqueous electrolytes at 25 °C: $NaClO_3$, $NaClO_4$, $NaNO_3$, NaBr O_3, $NaIO_3$, $KClO_3$, $KBrO_3$, KIO_3, NH4NO_3, NH_4Cl, and NH_4ClO_4. *Can. J. Chem.* **56**, 24–28.

Rowland D., Königsberger E., Hefter G. and May P. M. (2015) Aqueous electrolyte solution modelling: some limitations of the Pitzer equations. *Appl. Geochem.* **55**, 170–183.

Rush R. M. (1988) Isopiestic measurements of the osmotic and activity coefficients for the system sodium perchlorate-barium perchlorate-water at 25 °C. *J. Chem. Eng. Data* **33**, 477–479.

Rush R. M. and Johnson J. S. (1968) Isopiestic measurements of the osmotic and activity coefficients for the systems $HClO_4$-$LiClO_4$-H_2O, $HClO_4$-$NaClO_4$-H_2O, and $LiClO_4$-$NaClO_4$-H_2O. *J. Phys. Chem.* **72**, 767–774.

Rush R. M. and Johnson J. R. (1971) Isopiestic measurements of the osmotic and activity coefficients for the systems $HClO_4 + UO_2(ClO_4)_2 + H_2O$ and $NaClO_4 + UO_2(ClO_4)_2 + H_2O$ at 25 °C. *J. Chem. Thermodyn.* **3**, 779–793.

Stevenson A., Burkhardt J., Cockell C. S., Cray J. A., Dijksterhuis J., Fox-Powell M., Kee T. P., Kminek G., McGenity T. J., Timmis K. N., Timson D. J., Voytek M. A., Westall F., Yakimov M. M. and Hallsworth J. E. (2015) Multiplication of microbes below 0.690 water activity: implications for terrestrial and extraterrestrial life. *Environ. Microbiol.* **17**, 257–277.

Stillman D. E., Michael T. I., Grimm R. E. and Hanley J. (2016) Observations and modeling of northern mid-latitude recurring slope lineae (RSL) suggest recharge by a present-day martian briny aquifer. *Icarus* **265**, 125–138.

Stokes R. H. and Levien B. J. (1946) The osmotic and activity coefficients of zinc nitrate, zinc perchlorate and magnesium perchlorate. transference numbers in zinc perchlorate solutions. *J. Am. Chem. Soc.* **68**, 333–337.

Toner J. D., Catling D. C. and Light B. (2014a) The formation of supercooled brines, viscous liquids, and low temperature perchlorate glasses in aqueous solutions relevant to Mars. *Icarus* **233**, 36–47.

Toner J. D., Catling D. C. and Light B. (2014b) Soluble salts at the Phoenix Lander site, Mars: a reanalysis of the Wet Chemistry Laboratory data. *Geochim. Cosmochim. Acta* **136**, 142–168.

Toner J. D., Catling D. C. and Light B. (2015a) Modeling salt precipitation from brines on Mars: evaporation versus freezing origin for soil salts. *Icarus* **250**, 451–461.

Toner J. D., Catling D. C. and Light B. (2015b) A revised Pitzer model for low-temperature soluble salt assemblages at the Phoenix Site, Mars. *Geochim. Cosmochim. Acta* **166**, 327–343.

Vanderzee C. E. and Swanson J. A. (1963) Heats of dilution and relative apparent molal enthalpies of aqueous sodium perchlorate and perchloric acid. *J. Phys. Chem.* **67**, 285–291.

Associate editor: Jeffrey G. Catalano